



De-risk Breadboarding Activities on Regolith Transport

Final Report
02 April – 31 January 2020

Technical University of Munich
Institute of Aeronautics

Laura Grill

Contents

1	Meetings	6
2	Task description	7
3	Work Package Progress	8
3.1	Proof of concept for sample transport with vibrated conveyer under vacuum.....	8
3.1.1	Test setup design	8
3.1.2	Test setup manufacturing, improvement and activation	10
3.1.3	Proof of concept vacuum tests	13
3.2	Parameter study for sample transport concept	14
3.2.1	Adjustment/Enhancement of test setup	14
3.2.2	Experimental study with selected parameters	14
3.3	Feasibility of controlled hopper discharge	23
3.3.1	Adjustment/enhancement of test setup	23
3.3.2	Pre-tests	25
3.3.3	Experimental study with selected parameters	26
3.4	Simulant characterisation	29
3.4.1	Particle size distribution analysis of unprocessed	29
3.4.2	Shear tests of unprocessed and processed material.....	30
4	Design considerations for lunar environment.....	31
4.1	Hopper design	31
4.2	Conveyer design.....	31
5	References	33

List of figures

Figure 1: Prototype conveyors and covers made of stainless steel sheet metal for proof of concept testing	8
Figure 2: Sketch of the preliminary test setup for the conveyor (direction of vibration force highlighted red)	9
Figure 3: Concept sketch of common industrial vibratory conveyor driven by an electromagnetic actuator (Despotović et al., 2017)	10
Figure 4: Preliminary conveyor vacuum test setup	10
Figure 5: Conveyor vacuum test setup in vacuum chamber	11
Figure 6: Conveyor vacuum test setup with acrylic glass cover	11
Figure 7: Grounded conveyor vacuum test setup	12
Figure 8: Comparison of material behaviour in vacuum and ambient. Top: Material transport at ambient. Bottom: Material transport in vacuum	13
Figure 9: Test setup for conveyor parameter tests at ambient	14
Figure 10: Transportation times of 60 g NU-LHT-2M at 40 Hz and 0.5 mm stroke plotted over the angle of the direction of movement β depending on the angle of conveyor relative to horizontal with the ambient setup (shaker)	17
Figure 11: Transportation times of 60 g NU-LHT-2M with horizontal conveyor and stroke of 0.3 mm plotted over the angle of the direction of movement β and depending on the frequency with the vacuum setup (actuator) performed at ambient	17
Figure 12: Average time of sample transport and average sample mass flow depending on the sample mass with a horizontal conveyor. The plotted trend lines are quadratic	19
Figure 13: Conveying course for A: 10 g sample mass, B: 20 g sample mass, C: 40 g sample mass, D: 100 g sample mass	20
Figure 14: Conveying course for 150 g sample mass	20
Figure 15: Particle size distribution of NU-LHT-2M adopted from Zeng et al. (Zeng, He and Wilkinson, 2010), of BP-1 adopted from Rahmatian and Metzger (Rahmatian and Metzger, 2010) and of lunar soil average adopted from Zeng et al. (Zeng, He and Wilkinson, 2010)	21
Figure 16: Acrylic glass cover after test run with no visible clouding caused by material adhesion	22
Figure 17: Hopper wall angles	23
Figure 18: A: Sketch of the preliminary test setup for the hopper with continuous filling. B: Sketch of the improved test setup for the hopper with continuous filling.	24
Figure 19: A: Preliminary test setup for hopper discharge tests. B: Improved test setup for hopper discharge tests with continuous filling. C: Test setup for hopper discharge tests with a not axisymmetric setup	24
Figure 20: Sketch of the setup for parameter studies for hopper discharge tests. A: Investigation of the influence of radial offset from the hopper central axis. B: Investigation of the influence of a not axisymmetric setup	24
Figure 21: Residual fraction $m_{\text{hopper}}/m_{\text{total}}$ in the flat hopper (hopper 1) plotted over the tilting time of the shovel for different radial offsets from the hopper central axis	26
Figure 22: Mean residual fraction value of the grounded and not grounded setup with error bars in the flat hopper depending on the discharge rate	29
Figure 23: Particle size distribution of NU-LHT-2M measured by TUM and Zeng et al. (Zeng, He and Wilkinson, 2010) and of lunar soil average adopted from Zeng et al. (Zeng, He and Wilkinson, 2010)	30

Figure 24: Possible design concept for uphill regolith transportation with multiple vibratory conveyors.....	32
Figure 25: Possible design concept for uphill regolith transportation using a sawtooth texture (figure taken from (Chen et al., 2019)).....	32

List of tables

Table 1: Task description of the de-risk breadboarding activities on regolith transport performed at TUM	7
Table 2: Design envelope for the conveyer.....	9
Table 3: Test setup parameters for conveyer vacuum feasibility tests	11
Table 4: Possible settings of shaker and conveyer angles	14
Table 5: Results of the parameter study of different conveyer geometries with altering frequencies and strokes.....	15
Table 6: Time of sample transport for different conveyer inclinations.....	16
Table 7: Transported sample mass for different conveyer inclinations	16
Table 8: Time of sample transport for different actuator inclinations and frequencies with a horizontal conveyer	16
Table 9: Time of sample transport and transported sample mass for different initial sample masses	19
Table 10: Time of sample transport for different material and frequencies with a horizontal conveyer	20
Table 11: Time of sample transport of 60 g NU-LHT-2M for different frequencies with a horizontal conveyer in vacuum compared to the same experimental run at ambient	22
Table 12: Design envelope for the hopper	23
Table 13: Results of residual sample mass in the hopper measured for hopper discharge pre-tests (n.m.: not measurable)	25
Table 14: Residuals in the different hoppers after discharge.....	25
Table 15: Residual fraction ($m_{\text{hopper}}/m_{\text{total}}$) in the hopper 1 depending on the tilting time of the shovel and the radial offset from the hopper central axis.	27
Table 16: Residual fraction ($m_{\text{hopper}}/m_{\text{total}}$) in the hopper 2 depending on the tilting time of the shovel and the radial offset from the hopper central axis.	27
Table 17: Residual fraction ($m_{\text{hopper}}/m_{\text{total}}$) in the hopper 3 depending on the tilting time of the shovel and the radial offset from the hopper central axis.	27
Table 18: Residual fraction ($m_{\text{hopper}}/m_{\text{total}}$) in the hopper 3 depending on the lower wall angle in relation to horizontal.	28
Table 19: Residual fraction ($m_{\text{hopper}}/m_{\text{total}}$) in the hopper 1 depending on the tilting time of the shovel. Results from both grounded and not grounded setup can be compared.	28
Table 20: Important values for NU-LHT-2M determined with dynamic image analysis and laser diffraction.....	30

1 Meetings

The following meetings have been convened in the reporting period:

Date	Location	Description	Participants
2 April 2019	Teleconference	Kick-off	TUM, OHB-D, OHB-I
10 May 2019	Teleconference	Progress meeting	TUM, OHB-D
22 July 2019	TU Munich	Progress meeting	TUM, OHB-D, OHB-I
19 August 2019	Teleconference	Progress meeting	TUM, OHB-D
11 October 2019	Teleconference	Progress meeting	TUM, OHB-D
28 October 2019	Teleconference	Progress meeting	TUM, OHB-D
27 November 2019	Teleconference	Progress meeting	TUM, OHB-D
8 January 2020	Teleconference	Progress meeting	TUM, OHB-D
13 January 2020	TU Munich	Progress meeting	TUM, OHB-D
17 January 2020	Teleconference	Progress meeting	TUM, OHB-D, OHB-I

2 Task description

Table 1: Task description of the de-risk breadboarding activities on regolith transport performed at TUM

ID	Title	Task	Description
1.1	Basic prove of concept for sample transport with vibrated conveyer under vacuum	Test setup design	The general feasibility of transporting a sample under vacuum with a vibrated is evaluated.
1.2		Test setup manufacturing	
1.3		Proof of concept vacuum tests	
2.1	Parameter study/ sensitivity study on relevant parameters for sample transport concept	Adjustment/enhancement of test setup	A more detailed analysis of the sample transport with respect to selected influence parameters is conducted to allow the derivation of general design rules. Investigated influence parameters are: <ul style="list-style-type: none"> - Sample type - Sample particle size (distribution) - Sample mass - Vibration frequency - Vibration amplitude - Electrical grounding of conveyer - Inclination angle of conveyer - Angle between conveyer and actuator
2.2		Experimental studies with selected parameters	Output parameters determined through test include: <ul style="list-style-type: none"> - Sample transport rate along conveyer (g/s) - Degree of dust contamination in conveyer - Particle size sorting effects (alteration of PSD through transport)
3.1	Feasibility of controlled hopper discharge	Adjustment/enhancement of test setup	The hopper properties required to maintain a continuous, controlled flow rate are determined. Investigated influence factors are: <ul style="list-style-type: none"> - Sample mass - Hopper wall angle - Hopper geometry/setup symmetry - Sample discharge rate - Discharge position of the sample - Electrical grounding of hopper
3.2		Experimental studies with selected parameters	The ideal flow rate is determined through the transport capabilities of the conveyer, i.e. the amount of sample that can be processed (transport rate). The discharge rate shall equal the transport rate to maintain a constant sample layer thickness on the conveyer. Output parameters to be determined through test include: <ul style="list-style-type: none"> - Sample residuals in hopper - Discharge modes for controlled sample transport
4.1	Simulant characterisation	Shear/penetration test of unprocessed material	The simulant used for the ISRU demonstrator shall be characterised before and after processing to evaluate the effect of the chemical reduction process on the sample properties. Relevant sample properties that are expected to be altered through chemical reduction are the particle morphology, friction angle, cohesion, and particle size distribution (PSD). It is therefore planned to take subsamples of the original and processed simulant feedstock and characterise/analyse them in respective laboratories.
4.2		PSD analysis of unprocessed material	
4.3		Shear/penetration test of processed material	
4.4		PSD analysis of processed material	

3 Work Package Progress

3.1 Proof of concept for sample transport with vibrated conveyer under vacuum

3.1.1 Test setup design

a) Conveyer concept design

Vibratory conveyors have many advantages when it comes to automatic and continuous material transport of lunar regolith for ISRU applications. One major advantage compared to belt conveyors is the potentially simple design, the low energy consumption and the possibility to manufacture the trough from heat- and corrosion-resistant material. (Zhao, Huang and Zhao, 2013) This is why the concept of a vibratory conveyer was chosen for this study.

Pre-tests were performed with the shaker located at the Chair of Astronautics at TUM, which uses a sinus signal. According to Chen et al. (2019), an excitation parallel to the axis of the conveyer trough is only possible with non-sinusoidal vibration (shock) or with the help of an appropriate surface structure, such as a sawtooth profile. Generally there are two different forms of transport on a linear conveyer: sliding (or slip principle) and oblique hopping (or micro throw principle) (El Hor et al., 2005; Nendel and Risch, 2010). Due to the form of the shaker signal and, for simplicity reasons, in the design of the conveyer trough, it was decided to design a conveyer setup using the micro throw principle. It occurs when the vertical component of acceleration is larger than the gravitational acceleration. To enable a gliding motion, the friction of the surface of the trough has to be overcome by the horizontal excitation force. In an ideal gliding transport, the material behaves like a fluid so that no dust is swirled up. In principle the movement of the material that shall be conveyed can be calculated mathematically. However, most mathematical descriptions of the problem include major simplifications, such as considering the entire sample as a single mass and neglecting particle interactions. In reality regolith is strongly polydisperse with different types of particle-particle interactions. Additionally, triboelectric effects will also occur, which complicate the pure analytical prediction of sample movement. Because of that, testing the conveyer with an appropriate regolith analogue in a relevant environment is inevitable.

b) Conveyer trough geometry and properties

It was decided to use a rectangular/planar conveyer rather than a tubular one because it is assumed that the degrees of freedom for mechanical agitation are greater with a planar conveyer. It also simplifies the visual inspection of the material transport along the conveyer when using a transparent cover. The design envelope for the conveyer provided by OHB-I is summarized in Table 2, together with four prototypes that have been manufactured for early proof of concept studies. Each conveyer has a stainless steel cover plate to prevent dust contamination of the environment during testing (see Figure 1).



Figure 1: Prototype conveyers and covers made of stainless steel sheet metal for proof of concept testing

Table 2: Design envelope for the conveyer

Dimension	Envelope	Conveyer 1 (standard)	Conveyer 2 (short)	Conveyer 3 (thin)	Conveyer 4 (narrow)
Width	10 – 50 mm	50 mm	50 mm	50 mm	25 mm
Length	150 – 250 mm	250 mm	150 mm	250 mm	250 mm
Height	10 – 50 mm	40 mm	40 mm	40 mm	40 mm
Inclination (vs. horizontal)	-45 – +45 deg	adjustable	adjustable	adjustable	adjustable
Wall thickness	0.2 – 3.0 mm	1.0 mm	1.0 mm	0.5 mm	1.0 mm
Material	stainless steel	stainless steel 304	stainless steel 304	stainless steel 304	stainless steel 304
R _a		0,124 µm	0,112 µm	0,076 µm	0,127 µm
R _z		1,375 µm	1,366 µm	0,703 µm	1,413 µm

c) Ambient test setup

Figure 2 shows a sketch of the test setup with the conveyer mounted on a tiltable TIRA 51140 shaker. The shaker has a frequency range of 2 – 6500 Hz, a maximum displacement of 20 mm, and a maximum acceleration of 100 g. The angle α can be adjusted to investigate different inclinations for material transport and the angle β can be adjusted to test different directions of the vibration axis, or the excitation force on the conveyer trough respectively. The angle β is typically around 25° – 30° for conventional vibratory conveyors. Typical values found for the sinusoidal vibration frequency of common (larger) vibratory conveyors are < 100 Hz with amplitudes < 20 mm. This range is well covered with the shaker that was employed for the initial feasibility tests and the parameter study with the ambient setup.

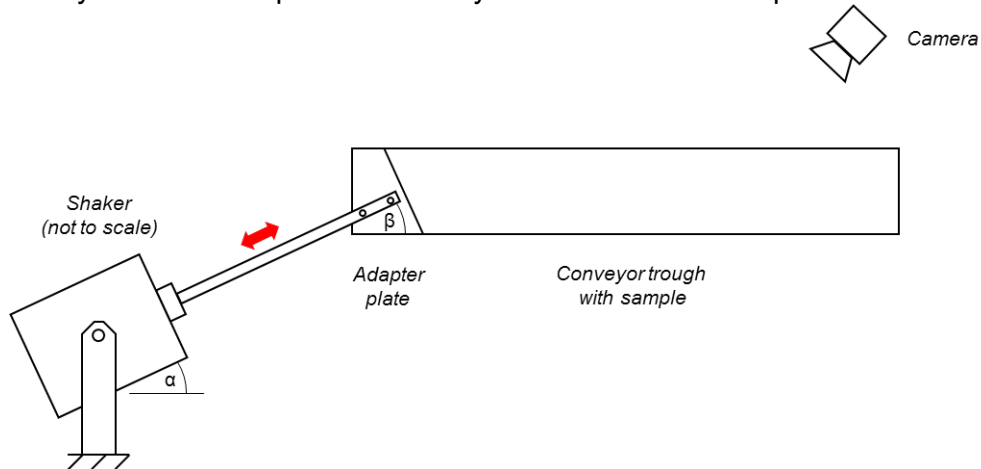


Figure 2: Sketch of the preliminary test setup for the conveyer (direction of vibration force highlighted red)

d) Vacuum test setup

For the vacuum tests, the shaker is replaced with an amplified piezoelectric actuator and the conveyer trough is supported by leaf springs mounted on a baseplate, similar to the design shown in Figure 3. The conveyer trough used for vacuum tests is conveyer 1 (see Table 2). The actuator used for the vacuum test setup is the FPA-1000E-P-1054-150-SS-1M4 FlexFrame PiezoActuator™ from Dynamic Structures & Materials, LLC. The spring plate used for the leaf springs is 0.5 mm thick, 50 mm in width, and 105 mm in length. The preliminary vacuum setup is depicted in Figure 4.

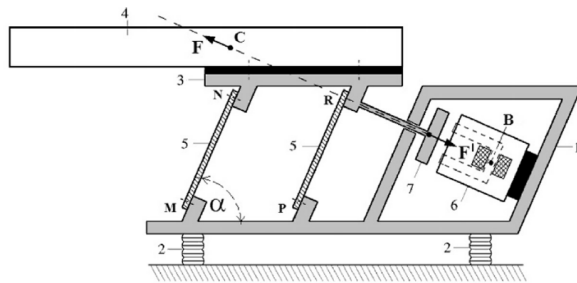


Figure 3: Concept sketch of common industrial vibratory conveyer driven by an electromagnetic actuator (Despotović et al., 2017).

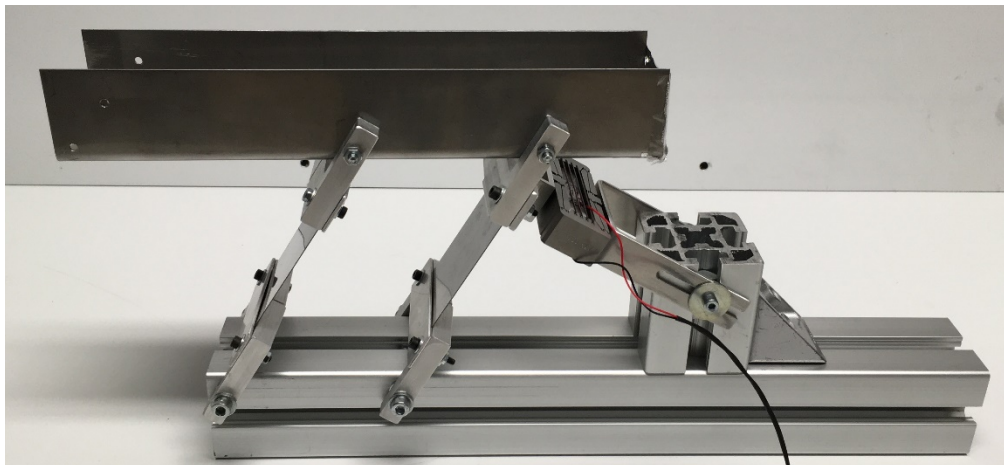


Figure 4: Preliminary conveyer vacuum test setup

3.1.2 Test setup manufacturing, improvement and activation

Results of the initial tests with the shaker as well as the actuator limitations informed the design of the vacuum breadboard with respect to the appropriate range of frequency, amplitude, and directivity of vibration. An intermediate piece has been added to cancel out shear and bending loads on the actuator. To monitor the actuator temperature and detect overheating in vacuum, a thermocouple has been mounted to the actuator. Also, after consulting the manufacturer, only positive voltages were used to avoid overheating in vacuum.

Since the loading of the conveyer system on the actuator was unknown and the displacement not only depends on the applied voltage but also on the loading, pre-tests with an acceleration sensor were performed. It was decided to operate the actuator conservatively, to prevent it from breaking due to overloading during the testing. The actuator operating settings were set to a voltage of 0 ± 2 V – 100 ± 5 V (analogue sine signal), resulting in a stroke of 0.3 mm, and frequencies between 40 ± 0.2 Hz and 45 ± 0.2 Hz. Test parameters for the tests performed in vacuum are summarized in Table 3.

To investigate potential clouding of a translucent cover due to particle adhesion, an acrylic glass cover was manufactured. Acrylic glass was chosen to investigate a “worst-case scenario”, because of its high susceptibility of triboelectric charging. The setup is depicted in Figure 6.

To investigate the influence of grounding of the setup, the conveyer was connected to a bolt, which was connected to the grounded base plate of the vacuum chamber. This setup is depicted in Figure 7.

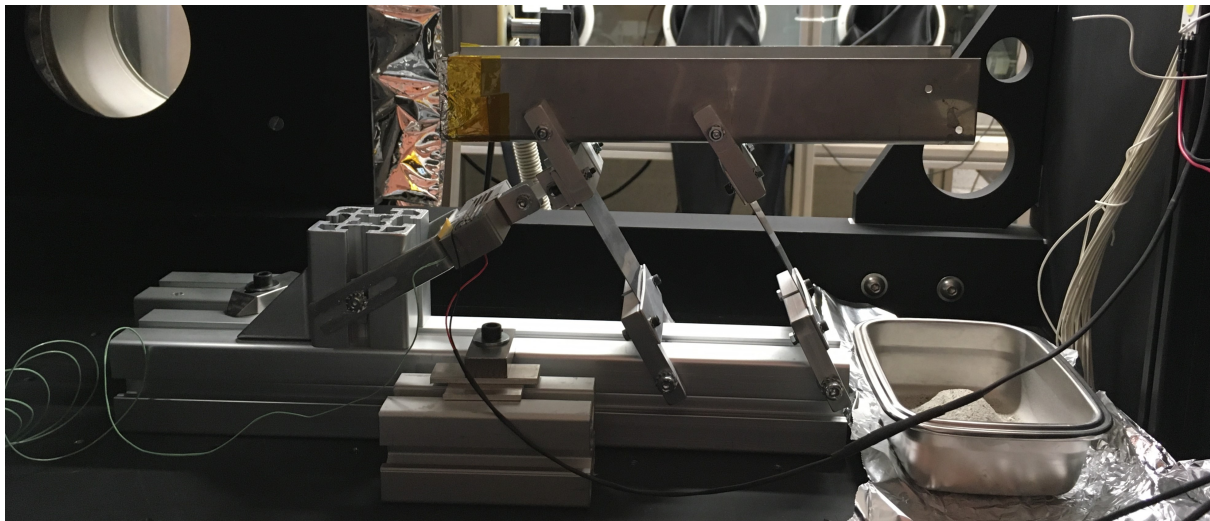


Figure 5: Conveyer vacuum test setup in vacuum chamber

Table 3: Test setup parameters for conveyer vacuum feasibility tests

Conveyer trough geometry (WxLxH)	50 mm x 250 mm x 40 mm
Conveyer inclination	0° (horizontal)
Angle α	30°
Angle β	30°
Signal type	Sine
Voltage	0 V – 100 V
Stroke	0.3 mm
Frequency	40 Hz, 42 Hz, 45 Hz

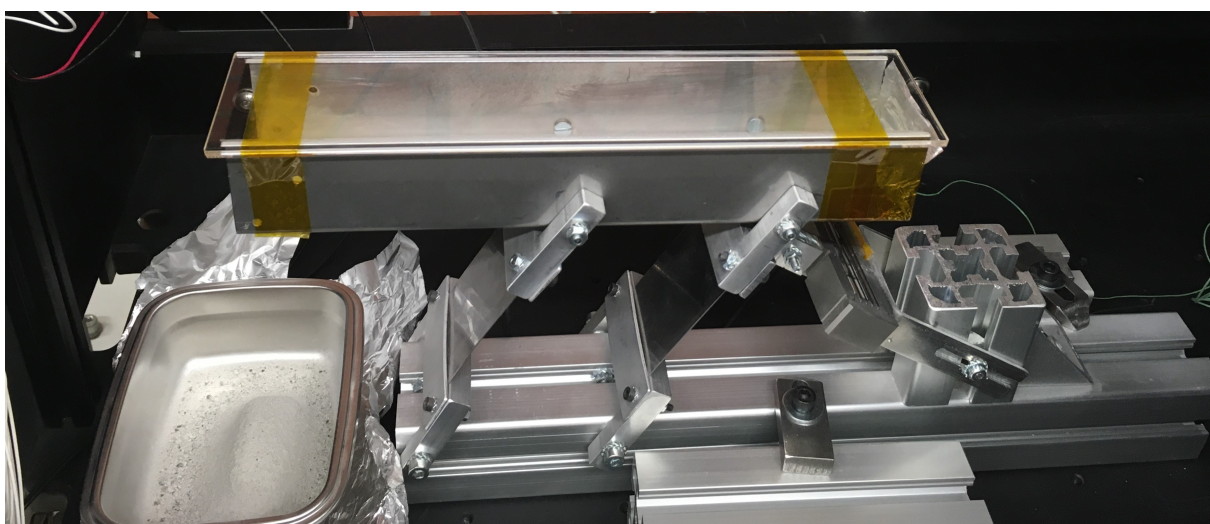


Figure 6: Conveyer vacuum test setup with acrylic glass cover

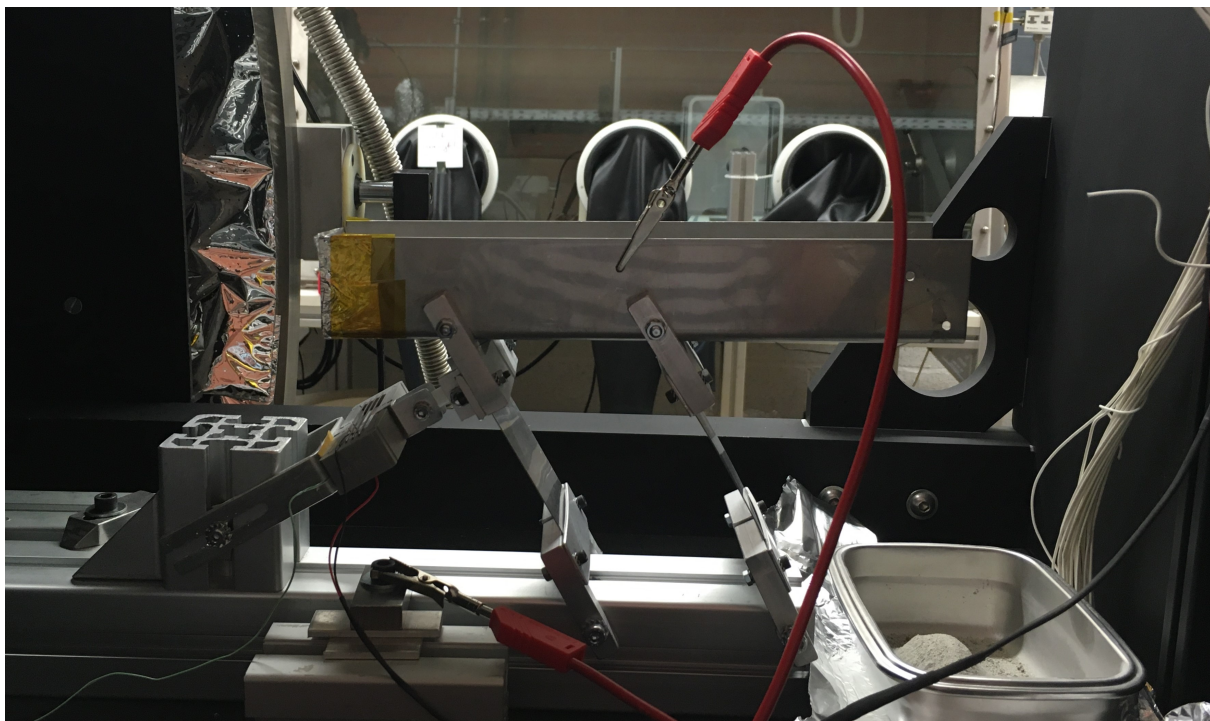


Figure 7: Grounded conveyer vacuum test setup

3.1.3 Proof of concept vacuum tests

Feasibility of material transport with a vibrated conveyer could be demonstrated. 60 g of the lunar regolith simulant NU-LHT-2M (standard particle size distribution) could be conveyed without restraints in the investigated test cases. Behavioural differences could be observed between material conveying in vacuum and reference measurements at ambient. While the surface of the conveyed material at ambient is smooth during the whole conveying process, it shows wave-like structures when conveyed in vacuum (see Figure 8; left column).

When material is conveyed at ambient conditions, residuals accumulate in the gap at the back-end of the trough. These residuals are released little by little during the conveying process and are conveyed as small discontiguous accumulations after the material bulk (see Figure 8; top right). In contrast, the conveyed material in vacuum forms a sharp line and no such residuals can be observed (see Figure 8, bottom right).

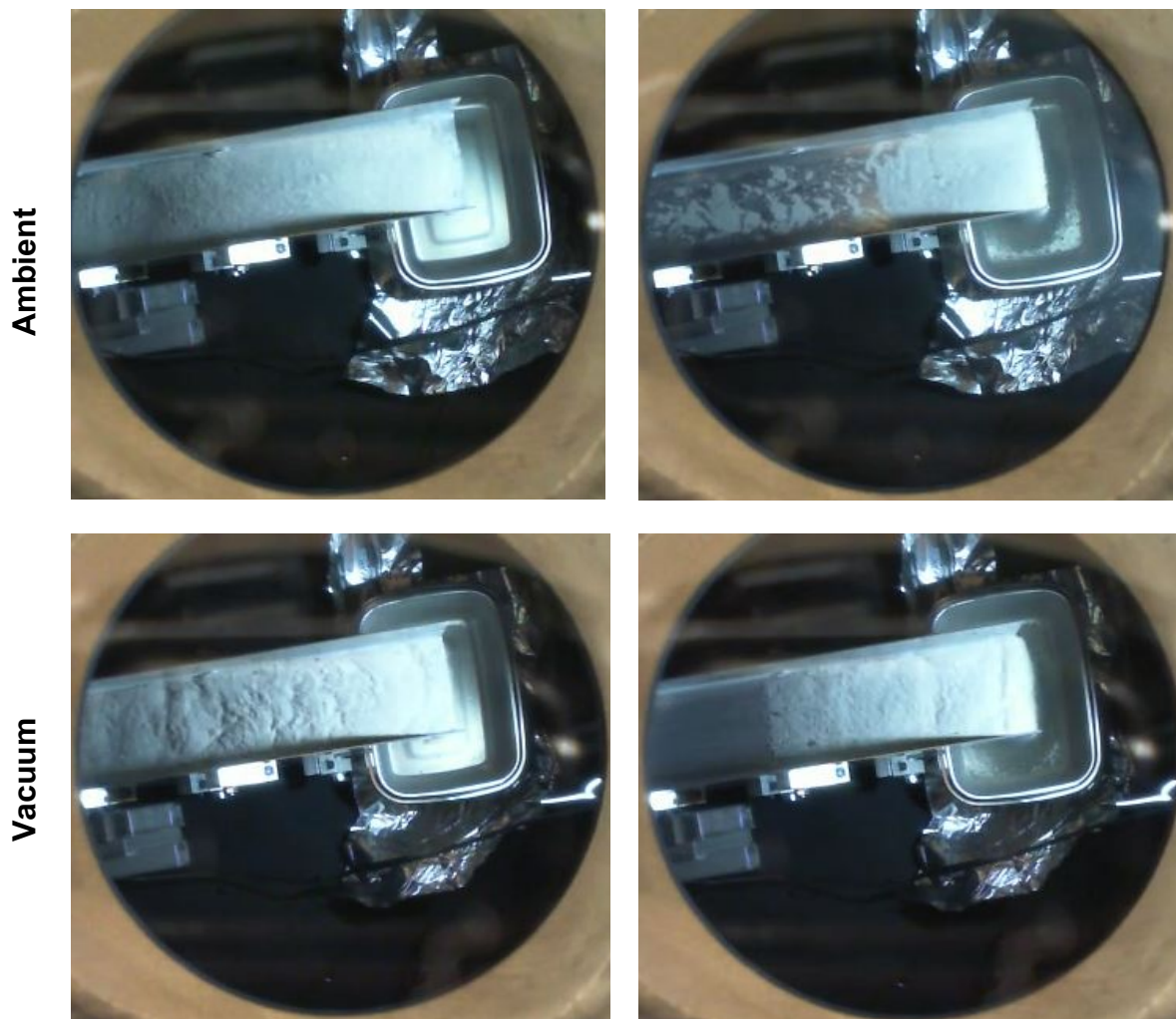


Figure 8: Comparison of material behaviour in vacuum and ambient. Top: Material transport at ambient. Bottom: Material transport in vacuum

3.2 Parameter study for sample transport concept

3.2.1 Adjustment/Enhancement of test setup

An adapter has been designed and manufactured to be able to mount the different conveyors on the shaker at different angles relative to the direction of movement of the shaker. The direction of movement of the shaker can be set to angles between -90° and +90° relative to the horizontal. The adapter between shaker and conveyor allows settings as summarized in Table 4. The test setup is depicted in Figure 9.

Table 4: Possible settings of shaker and conveyor angles

α	Conveyor angle to horizontal		
	-15°	0°	15°
15°	yes	yes	no
30°	yes	yes	yes
45°	yes	yes	yes

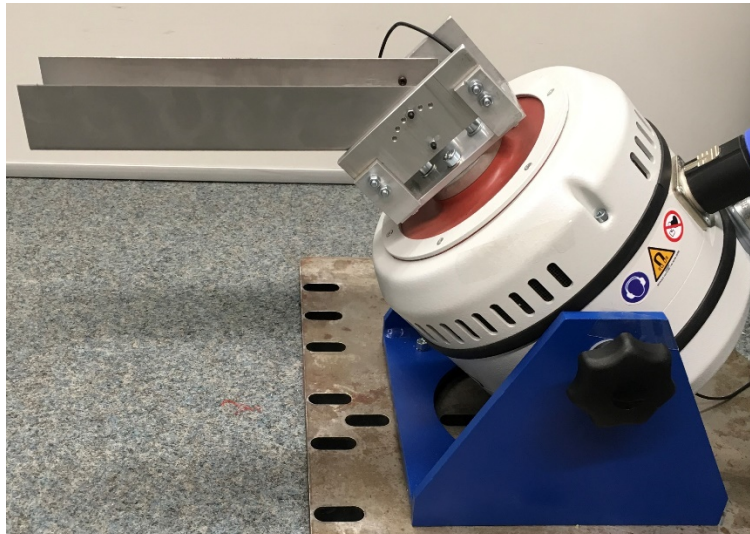


Figure 9: Test setup for conveyor parameter tests at ambient

3.2.2 Experimental study with selected parameters

Basic feasibility of the transport mechanism as well as parameter studies were performed with the conveyors described in Table 2 and Figure 1. For this purpose, the test setup depicted in Figure 9 was employed to evaluate different modes and directions of vibration for variably inclined conveyors. Investigated parameters as well as parameter study results are described in the following sections.

3.2.2.1 Frequency and stroke

The parameter study with altering frequencies and strokes was performed with 60 g of the lunar regolith simulant NU-LHT-2M (standard particle size distribution) at ambient conditions. The shaker angle is set to 30° from horizontal and the conveyor angle is 0° from horizontal. Details on the investigated conveyors can be taken from Table 2.

Investigated frequencies are 30 Hz, 40 Hz, 50 Hz, 60 Hz, and 70 Hz, and investigated strokes are 0.1 mm, 0.3 mm, and 0.5 mm. Transportation times of the sample for the investigated frequencies and strokes can be found in Table 5

Based on the results, default parameters were chosen to be set to 40 Hz frequency and 0.3 mm – 0.5 mm stroke.

Table 5: Results of the parameter study of different conveyer geometries with altering frequencies and strokes

		standard conveyor			thin conveyor		
		Stroke			Stroke		
Time of transport [s]		0.1 mm	0.3 mm	0.5 mm	0.1 mm	0.3 mm	0.5 mm
Frequency	30 Hz	-	-	-	-	-	-
	40 Hz	-	19,5	9,8	-	9,4	5,0
	50 Hz	-	-	-	98,0	22,0	23,1
	60 Hz	-	-	-	-	-	-
	70 Hz	-	16,3	5,2	-	-	-

		short conveyor			narrow conveyor		
		Stroke			Stroke		
Time of transport [s]		0.1 mm	0.3 mm	0.5 mm	0.1 mm	0.3 mm	0.5 mm
Frequency	30 Hz	-	45,0	10,0	-	194 (482)*	26,0
	40 Hz	-	11,0	3,7	-	11,6	11,5
	50 Hz	256,0	4,0	2,5	-	-	-
	60 Hz	33,0	11,0	1,8	-	67 (105)**	-
	70 Hz	-	-	-	106,0	-	-

Legend	
 	Sample does not move or only very slowly -> abort
 	99,99 Sample experiences nonlinear motion caused by vibration in natural frequency of the conveyer -> delayed emptying
 	- Sample experiences nonlinear motion caused by vibration in natural frequency of the conveyer -> no transport, abort
*	Value in brackets caused by delayed emptying due to material sticking to the walls
**	Value in brackets caused by delayed emptying of the trough due to material accumulation near the edge

3.2.2.2 Conveyer angles

The parameter study with different conveyer and shaker angles was performed with 60 g of the lunar regolith simulant NU-LHT-2M (standard particle size distribution) at ambient conditions. Based on the results of the previously performed parameter study (see 3.2.2.1), the frequency was set to 40 Hz and the stroke to 0.5 mm. The conveyer that was used is conveyer 1 (see Table 2).

Investigated shaker angles are 15°, 30°, and 45° from horizontal, and investigated conveyer angles are -15°, 0°, and 15° from horizontal. The measurement with the shaker angle/conveyer angle combination of 15°/15° could not be carried out because the adapter between the shaker and the conveyer was not designed for this setting. Transportation times of the sample as well as the overall transported sample mass for the investigated inclination angles can be found in Table 6 and Table 7.

The most important outcome of this parameter study is that sample transport is also feasible uphill. As expected, the time of transport is the shortest when the transportation direction of the sample is downhill and increases with an increasing conveyer angle. Also, for this setup and the chosen settings, the more acute the angle β is, the faster is the material transport.

Material loss during experiments is due to residuals of fines in the conveyer and loss of fines for the test runs with conveyer angles of -15° and 0° and additionally residuals of very coarse particles in the conveyer for conveyer angles of 15°.

Table 6: Time of sample transport for different conveyer inclinations

Time of transport [s]		Conveyer angle		
		minus 15°	0°	15°
Shaker angle	15°	3,7	3,9	
	30°	4,2	8,4	7,9
	45°	5,4	9,1	11

Table 7: Transported sample mass for different conveyer inclinations

Mass after test [g]		Conveyer angle		
		minus 15°	0°	15°
Shaker angle	15°	59,7	59,6	
	30°	59,7	59,4	56,1
	45°	59,6	59,2	54,7

Test runs with different β angles and with a horizontal conveyer have been repeated with the vacuum setup described in 3.1.2 and depicted in Figure 5. The stroke was set to 0.3 mm and frequencies of 40 Hz, 42 Hz, and 45 Hz where investigated. The angle β was set to 20°, 30°, and 45° to investigate its influence on particle transportation. Results are summarized in Table 8.

Table 8: Time of sample transport for different actuator inclinations and frequencies with a horizontal conveyer

Time of transport [s]		Frequency		
		40 Hz	42 Hz	45 Hz
Actuator angle β	20°	26	19	14
	30°	17,6	14,3	11,6
	45°	19	16	12

Transportation times are plotted over the angle of the direction of movement relative to the conveyer β for the different sets of experiments described above. Figure 10 shows the results from Table 6. Linear trend lines are drawn for the different conveyer angle settings. It shows that the more acute the angle β is, the faster is the material transport. But also with increasing conveyer angle the slope of the trend line increases. This shows that the influence of the angle between the direction of movement and the conveyer is stronger when the conveyer angle is larger. For a downhill transportation (conveyer angle of -15°) the transportation time increases less with increasing angle β than for horizontal and uphill transportation, hence the angle β has less impact on the time of transportation.

Figure 11 shows the results from Table 8. Quadratic trend lines are drawn for the different frequency settings. This trend line type was chosen since it fits very well for all series. The diagram shows that transportation time decreases with increasing frequency for the same angle β in the investigated frequency interval. It also shows that for the here selected parameters the transportation time increases when the angle β becomes too acute or too wide. Contrary to the results of the experiments performed with the ambient setup with a stroke of 0.5 mm, there seems to be an optimum angle between the direction of movement and the conveyer, and the correlation “the more acute the angle β , the faster the material transport” is shown to be false. This is in accord with Chen et al., (2019), who state that an excitation parallel to the axis of the conveyer trough is only possible with non-sinusoidal vibration (shock) or with the help of an appropriate surface structure. The more acute the angle between the direction of movement and the conveying direction (i.e. the x-axis), the larger the vector part along the x-axis of the momentum vector and the wider the angle the larger the vector part along the z-axis. A large z-part results in high leaps of the particles but short path length, a large x-part results in low jumps but longer path length. It is about finding the optimum between x- and z-

parts of the momentum transfer, because a higher x-part also means less momentum transfer due to increased friction. Especially for smaller strokes this effect has a strong influence as the results show. For the vacuum setup at ambient with a stroke of 0.3 mm, the optimum of the angle β seems to be somewhere between 35° and 40°.

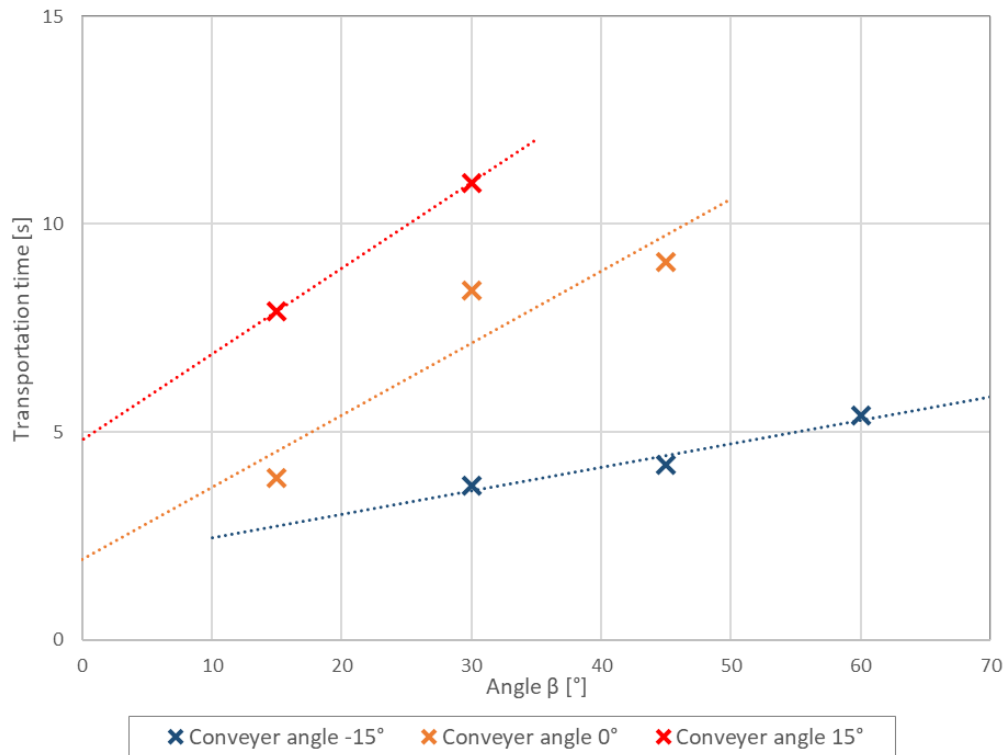


Figure 10: Transportation times of 60 g NU-LHT-2M at 40 Hz and 0.5 mm stroke plotted over the angle of the direction of movement β depending on the angle of conveyer relative to horizontal with the ambient setup (shaker).

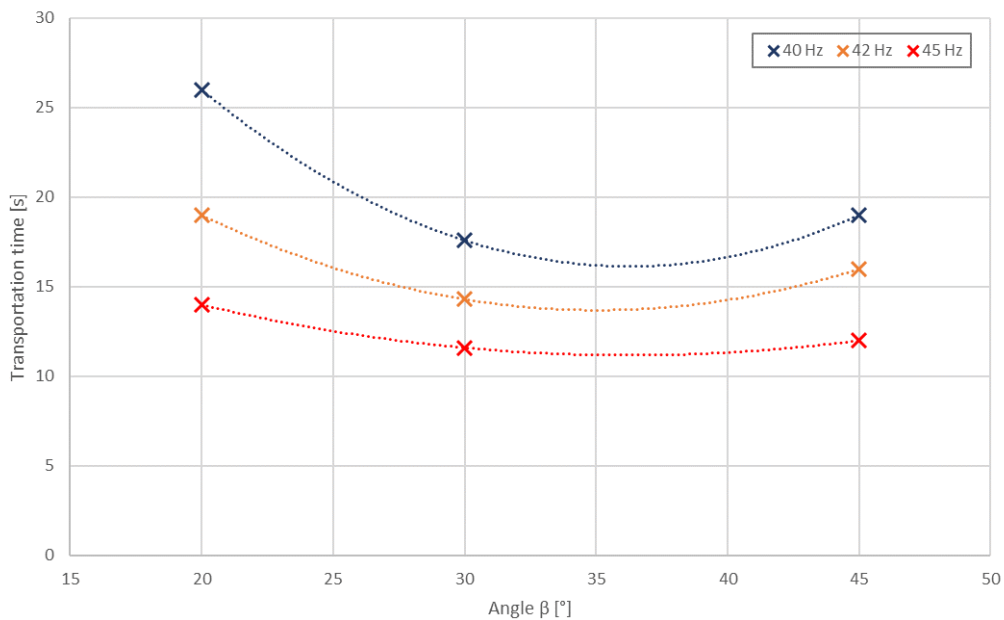


Figure 11: Transportation times of 60 g NU-LHT-2M with horizontal conveyer and stroke of 0.3 mm plotted over the angle of the direction of movement β and depending on the frequency with the vacuum setup (actuator) performed at ambient.

3.2.2.3 Sample mass

The parameter study with different initial sample masses was performed with the lunar regolith simulant NU-LHT-2M (standard particle size distribution) at ambient conditions. A test series with a horizontal conveyer was repeated with the setup described in 3.1.2 and depicted in Figure 5. The stroke was set to 0.3 mm, the frequency was 40 Hz, and the angle between the direction of movement and the conveyer was 30°. Initially performed experiments with the ambient test setup with the shaker (depicted in Figure 9) could not be evaluated due to irregularities in the experimental execution (sample was swirled up because of air draft, conveyer trough was slightly inclined leading to sample accumulation and conveying on only one side of the conveyer trough and not being evenly spread).

Investigated sample masses are 10 g, 20 g, 40 g, 60 g, 100 g and 150 g. Transportation times of the samples as well as the sample mass flow rates are summarized in Table 9. The calculated average transportation times for each investigated sample mass as well as the calculated average sample mass flow rates are plotted in Figure 12. Sample mass flow rate is calculated by measuring the time Δt between the sample first reaching the edge of the conveyer and when sample transport is completed. The sample mass flow rate \dot{m}_{sample} is then calculated as:

$$\dot{m}_{sample} = \frac{m_{sample}}{\Delta t}$$

The major outcome of this study is that the investigated system is also suitable for larger sample sizes than the default sample mass of 60 g. Also, the time of transport of the sample increases with increasing sample mass but not linearly (the shape of the plot suggests that there could be a quadratic correlation but further investigation is needed to better understand the correlations). The total time of transport is only marginally influenced by the time the sample needs to be conveyed to the edge of the conveyer trough. It takes 8-9 s for 10 g of sample to be conveyed to the edge of the trough and 5-6 s for 150 g of sample, depending on how the sample was filled in the trough in the first place. The shape of the sample mass flow rate curve is in accord with observations. For small sample sizes, the sample mass flow rate increases with increasing sample masses. This is due to the fact that the sample layer thickness of the conveyed sample increases as depicted in Figure 13. For small sample masses, the pile of simulant starts to spread while moving forward until the minimum sample layer thickness is reached. It is then evenly conveyed to the edge of the conveyer before falling off. For sample masses starting at 100 g the conveying course is different. The pile starts to spread but does not reach its minimum sample layer thickness before the material reaches the edge of the conveyer (see Figure 14 A and B). The pile is gradually skimmed while a thin layer of material is conveyed forward to the edge of the trough (Figure 14 C) and only when it has shrunk to a certain layer thickness the remaining material is evenly conveyed (Figure 14 D and E). This different conveying course seems to reduce the sample mass flow as the mass flow curve in Figure 12 shows. For a more fundamental and detailed interpretation of these observations, further investigation has to be conducted.

Table 9: Time of sample transport and transported sample mass for different initial sample masses

Sample mass [g]	Time of transport [s]	Average time of transport [s]	Sample mass flow [g/s]	Average sample mass flow [g/s]
10	13	12	2,5	2,5
	12		2,5	
	12		2,5	
20	13	13	4,0	3,8
	13		4,0	
	13		3,3	
40	16	16	5,0	4,6
	16		4,4	
	16		4,4	
60	19	18	6,0	5,7
	18		5,0	
	16		6,0	
100	24	24	5,6	5,6
	24		5,6	
	24		5,6	
150	37	39	4,8	4,5
	39		4,4	
	42		4,2	

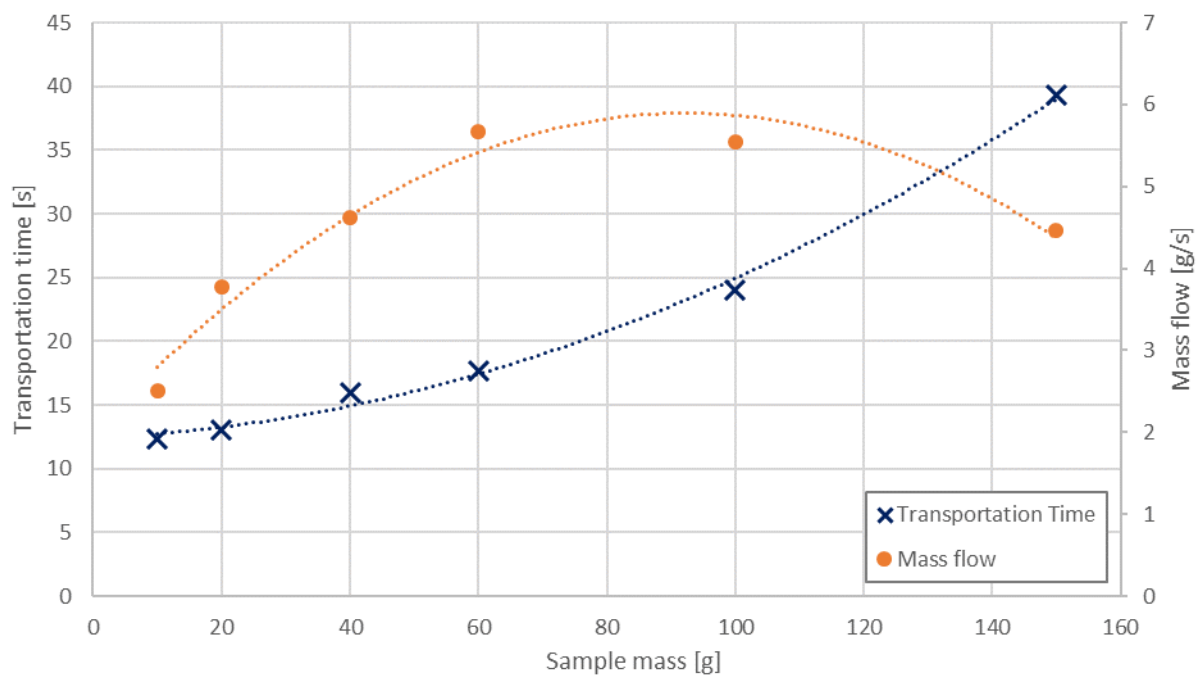


Figure 12: Average time of sample transport and average sample mass flow depending on the sample mass with a horizontal conveyer. The plotted trend lines are quadratic.

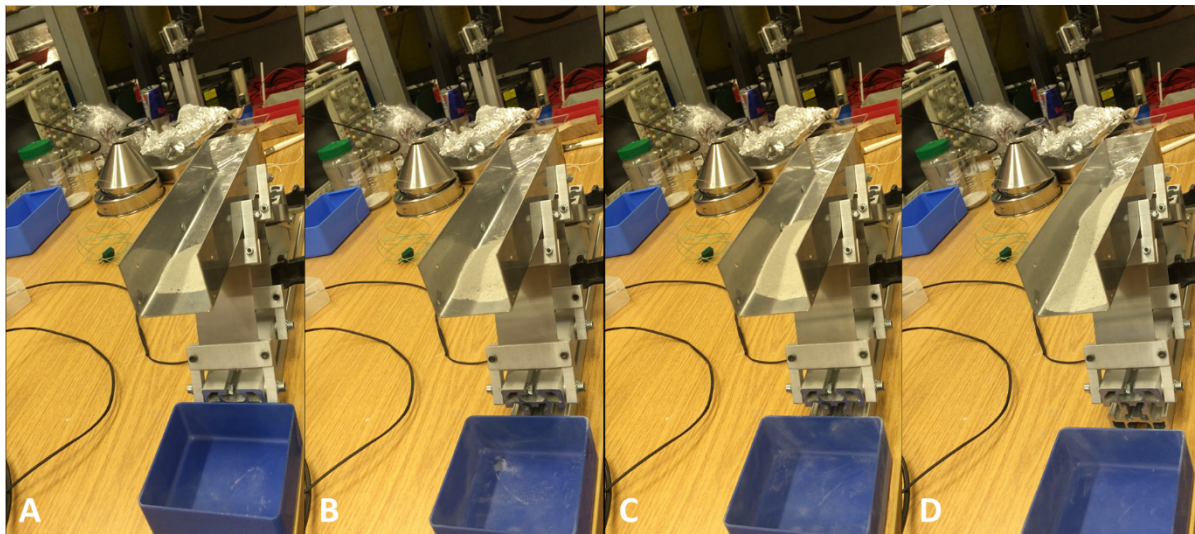


Figure 13: Conveying course for A: 10 g sample mass, B: 20 g sample mass, C: 40 g sample mass, D: 100 g sample mass.

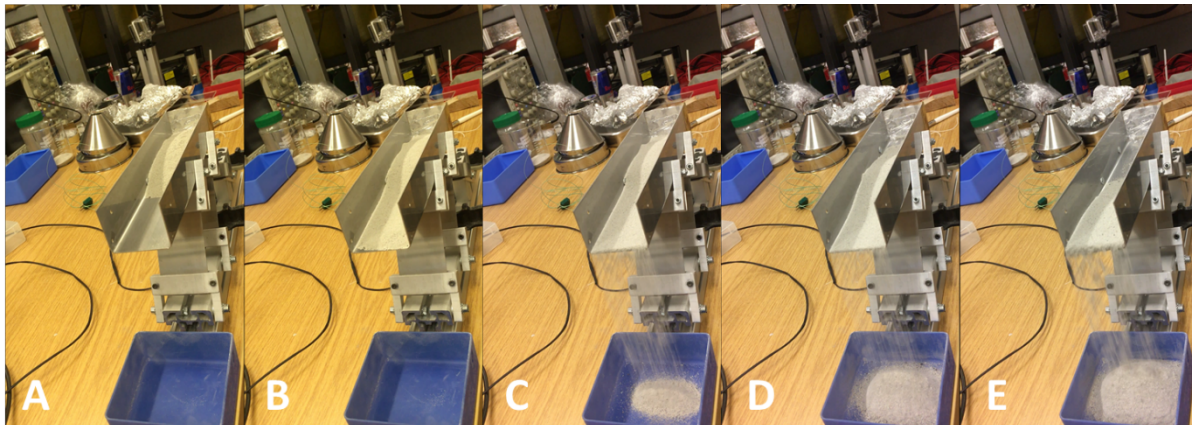


Figure 14: Conveying course for 150 g sample mass.

3.2.2.4 Particle size

Test runs with different material and with a horizontal conveyer have been performed with the vacuum setup described in 3.1.2 and depicted in Figure 5. The stroke was set to 0.3 mm and the angle between the direction of movement and the conveyer was 30°. Frequencies of 40 Hz, 42 Hz, and 45 Hz where investigated. The different materials that were used are NU-LHT-2M with its standard particle size distribution (see Figure 15 and 3.4.1), sieved NU-LHT-2M to a particle size fraction >125 µm, and BP-1 (see Figure 15). NU-LHT-2M sieved to the particle size fraction >125 µm is the coarsest of the investigated materials. BP-1 has a higher amount of very fine (<0.02 mm) and very coarse (>2 mm) particles than NU-LHT-2M. It also contains a few large chunks (several millimetres up to more than 1 cm). Results are summarized in Table 10.

Table 10: Time of sample transport for different material and frequencies with a horizontal conveyer

Time of transport [s]		Frequency		
		40 Hz	42 Hz	45 Hz
Material	NU-LHT-2M SPSD	17,6	14,3	11,6
	NU-LHT-2M >125µm	32	23	19
	BP-1	22	16	13

This validates for all materials that the time of sample transport increases when the frequency increases. The coarse fraction of NU-LHT-2M has remarkably longer transportation times than standard particle size NU-LHT-2M. This is in accordance with expectations, since path length per momentum transfer of coarser particles is smaller than for smaller particles due to their larger mass. Smaller path lengths lead to more leaps necessary to cover the distance, hence the longer transportation times for the coarse fraction.

BP-1 has slightly longer transportation times than NU-LHT-2M PSD. This could be due to the higher amount of very fine particles leading to more particle-particle and particle-wall friction. Also, fine particles might form larger agglomerates, effectively resulting in larger particles that have to be conveyed. The large chunks contained in the BP-1 simulant are also conveyed without constraints. They seem to be carried and dragged along by the bulk of small particles, floating on the upper layer of the conveyed material bulk. These large chunks might also contribute to the slower conveying speed of BP-1.

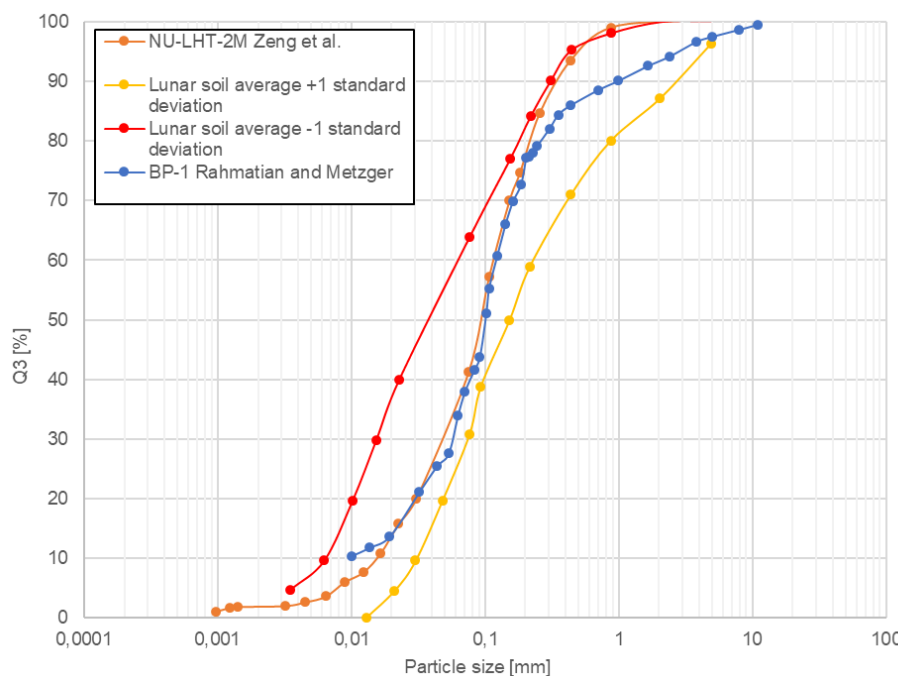


Figure 15: Particle size distribution of NU-LHT-2M adopted from Zeng et al. (Zeng, He and Wilkinson, 2010), of BP-1 adopted from Rahmatian and Metzger (Rahmatian and Metzger, 2010) and of lunar soil average adopted from Zeng et al. (Zeng, He and Wilkinson, 2010).

3.2.2.5 Vacuum

a) Influence of the frequency

Test runs with different frequencies with a horizontal conveyer have been performed in vacuum ($5 \cdot 10^{-4}$ mbar - $5 \cdot 10^{-3}$ mbar) with the setup described in 3.1.2 and depicted in Figure 5. The stroke was set to 0.3 mm and the angle between the direction of movement and the conveyer was 30°. Frequencies of 40 Hz, 42 Hz, and 45 Hz have been investigated. Results as well as reference values at ambient conditions are summarized in Table 11.

General feasibility of material transport with a vibrated conveyer was demonstrated, and material transport with the setup was as controllable and unproblematic in vacuum as at ambient. Time of transport is slower in vacuum than at ambient. The behaviour of the conveyed material in vacuum described in 3.1.3 suggests that its cohesive characteristics are more distinct in vacuum than at ambient. The fact that the material seems to move in one bulk and forms wavelike structures indicates that particles might form larger agglomerates and do not move as freely as at ambient. Also, particle-particle friction and particle-wall friction might be

higher in vacuum than at ambient due to the lack of air. This might also lead to slower transportation times in vacuum.

Table 11: Time of sample transport of 60 g NU-LHT-2M for different frequencies with a horizontal conveyer in vacuum compared to the same experimental run at ambient

Time of transport [s]		Frequency		
		40 Hz	42 Hz	45 Hz
Atmosphere	Ambient	17,6	14,3	11,6
	Vacuum	24	21	15

b) Dust contamination of translucent cover

A test run with a horizontal conveyer and a translucent cover of acrylic glass has been performed in vacuum ($5 \cdot 10^{-4}$ mbar - $5 \cdot 10^{-3}$ mbar) with the setup described in 3.1.2 and depicted in Figure 6. The stroke was set to 0.3 mm, the frequency was 40 Hz, and the angle between the direction of movement and the conveyer was 30°. Figure 16 shows the acrylic glass cover after the test run. No visible clouding caused by particle adhesion of the cover could be discerned. This is in agreement with previous observations of material behaviour during conveying tests in vacuum. Dust contamination of surfaces was generally less of an issue in vacuum than at ambient. This could be due to stronger particle-particle attraction in vacuum leading to previously described cohesive behaviour resulting in a stronger attraction between fines and the material bulk. Hence, particles – especially fines – might be less attracted by the trough surface than by other particles leading to less residuals of fines in the trough.



Figure 16: Acrylic glass cover after test run with no visible clouding caused by material adhesion

c) Grounding of the setup

A test run with a horizontal conveyer that was grounded has been performed in vacuum ($5 \cdot 10^{-4}$ mbar - $5 \cdot 10^{-3}$ mbar) with the setup described in 3.1.2 and depicted in Figure 7. The stroke was set to 0.3 mm, the frequency was 40 Hz, and the angle between the direction of movement and the conveyer was 30°. There was no difference between grounded and not grounded test runs in vacuum, neither in the behaviour of the conveyed material nor in the time of transport. This might be due to the choice of material (stainless steel) that was made because of its low susceptibility of triboelectric charging. Hence, there is probably no or no significant difference in built-up triboelectric charges between the two setups.

3.3 Feasibility of controlled hopper discharge

3.3.1 Adjustment/enhancement of test setup

It was decided to use conical hoppers rather than a square/rectangular hopper because of the risk of material/dust accumulation in edges. The design envelope for the hopper provided by OHB-I is summarized in Table 12. According to these specifications five different stainless steel hoppers were purchased and the three hoppers depicted in Figure 17 where chosen to be used for the feasibility study of controlled hopper discharge. The hopper dimensions are provided in Table 12. Certain deviations from the design envelope in terms of inlet diameter were accepted for the pre-tests because of availability issues. The steep and the flat hopper were used for pre-tests on sample flowability.

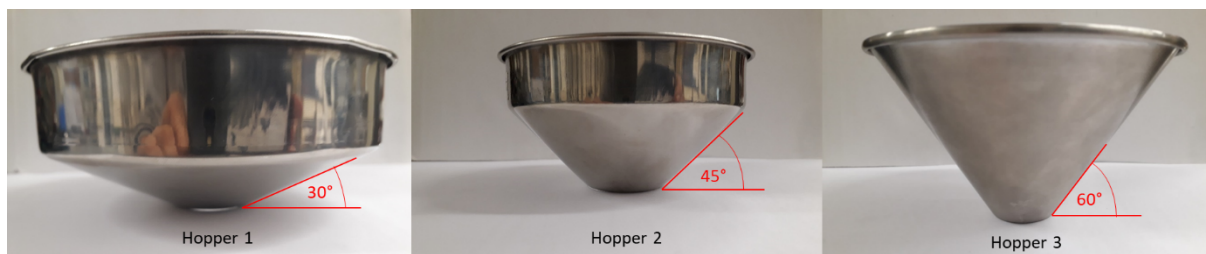


Figure 17: Hopper wall angles

Table 12: Design envelope for the hopper

Dimension	Envelope	Hopper 1 (flat)	Hopper 2 (standard)	Hopper 3 (steep)
Inlet diameter	80 mm	135 mm	98 mm	118 mm
Outlet diameter	15 – 35 mm	32	32 mm	26 mm
Wall angle (vs. horizontal)	30 – 70 deg	30 deg	45 deg	60 deg
Height	20 – 70 mm	56	54 mm	72 mm
Wall thickness	0.5 – 3.0 mm	1.0 mm	1.0 mm	1.0 mm
Material	stainless steel	stainless steel	stainless steel	stainless steel 304
R _a		0,484 µm	1,155 µm	0,376 µm
R _z		3,688 µm	8,431 µm	3,701 µm

Pre-tests on sample flow through these hoppers in vacuum with NU-LHT-2M were performed with the test setup depicted in Figure 18 A and Figure 19 A. The hopper guides the sample that is discharged by a shovel or similar to avoid spillage. For the vacuum tests, a manipulator feedthrough in the vacuum chamber was used to fill the sample into the hopper.

For parameter studies on hopper discharge in vacuum, the test setup has been improved and adapted as depicted in Figure 18 B. Contrary to the first setup, the sample discharge location does not move during one discharge run and the discharge rate is easier to control. Tests on the sample flow through the hoppers in vacuum were performed depending on the slope of the hopper walls, the discharge rate of the shovel, and the radial offset from the central axis where the shovel discharges the sample. The setup used for this parameter study is depicted in Figure 19 B and Figure 20 A. Furthermore, the results were compared to the test case where

the hopper is grounded. The same setup was used for the tests with a grounded setup but the hopper was connected to the vacuum chamber in order to ground it. Also, the influence of a not axisymmetric (perpendicular to the surface) setup was investigated. Figure 19 C and Figure 20 B depict the setup used for this parameter study.

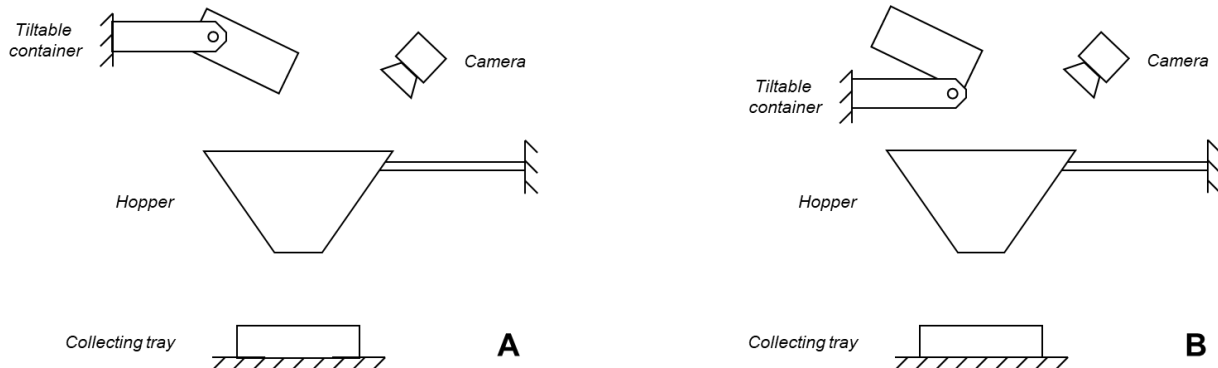


Figure 18: A: Sketch of the preliminary test setup for the hopper with continuous filling. B: Sketch of the improved test setup for the hopper with continuous filling.

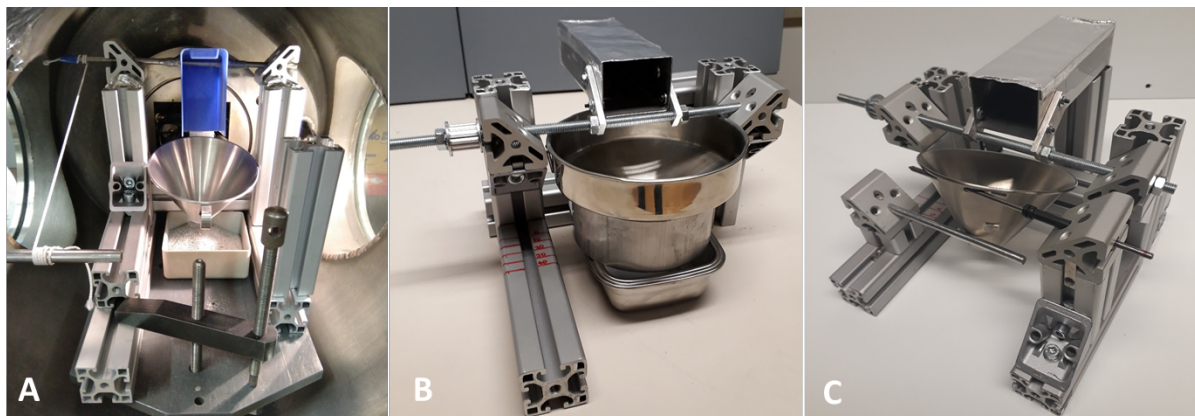


Figure 19: A: Preliminary test setup for hopper discharge tests. B: Improved test setup for hopper discharge tests with continuous filling. C: Test setup for hopper discharge tests with a not axisymmetric setup

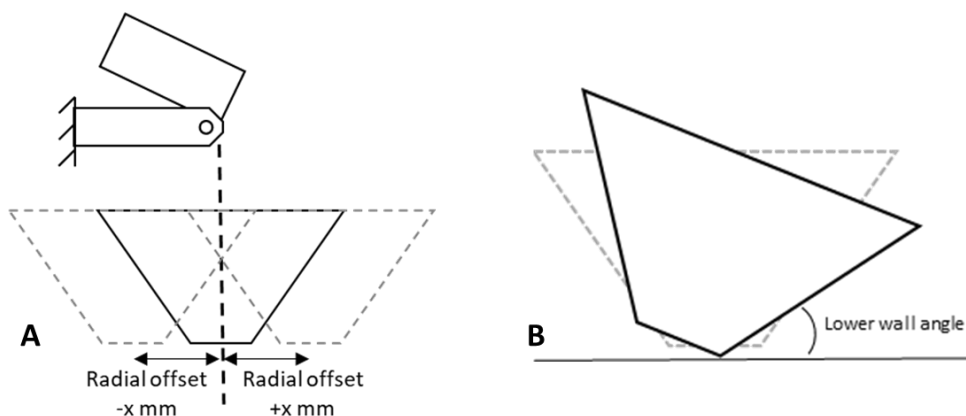


Figure 20: Sketch of the setup for parameter studies for hopper discharge tests. A: Investigation of the influence of radial offset from the hopper central axis. B: Investigation of the influence of a not axisymmetric setup

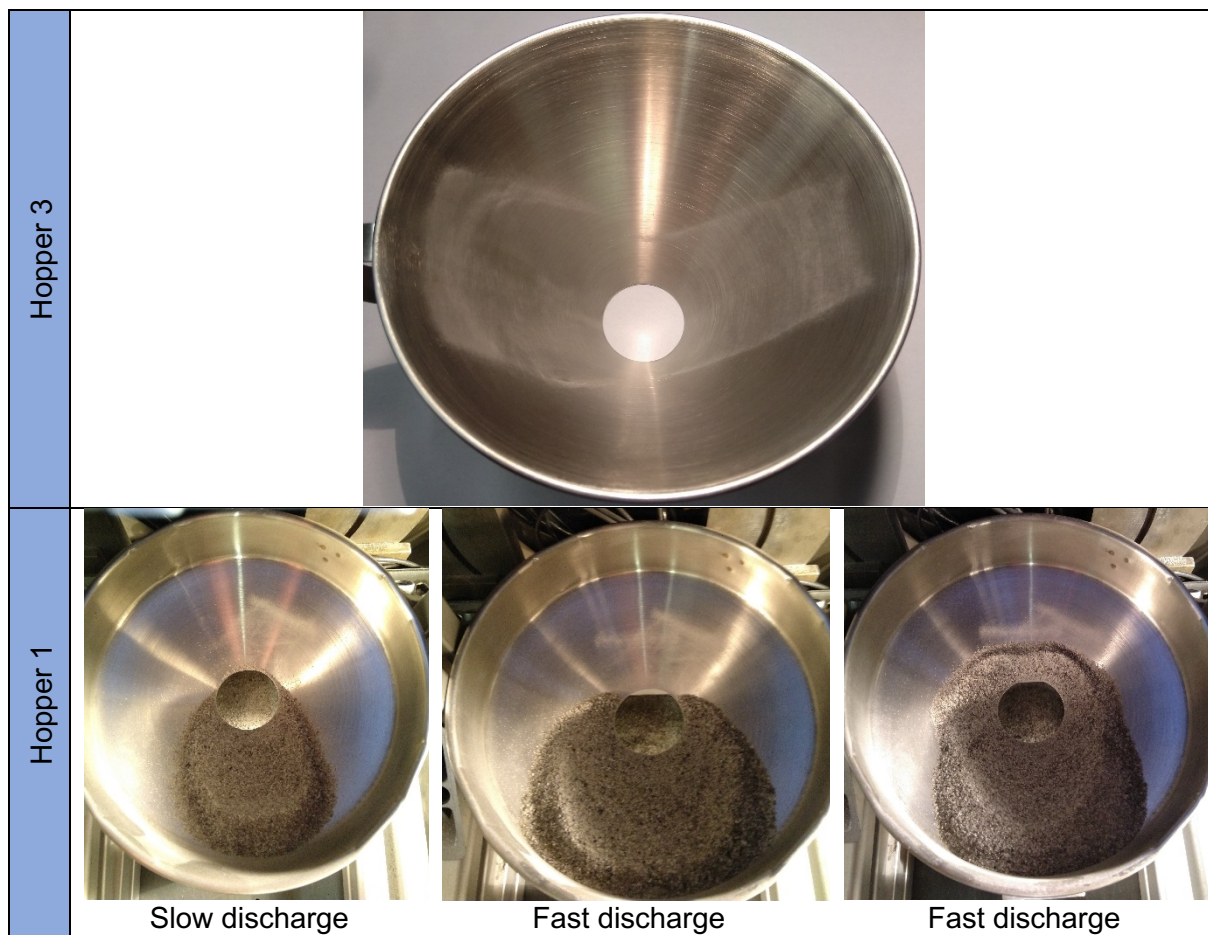
3.3.2 Pre-tests

Pre-tests for hopper discharge have been performed under vacuum with the lunar regolith simulant NU-LHT-2M (particle size $\geq 125 \mu\text{m}$). The default sample mass was 150 g. Pre-tests were performed with one steep and one flat hopper (for details see Hopper 1 and Hopper 3 in Table 12). For the steep hopper, only marginal residuals of fines stuck to the hopper surface after discharging. For the flat hopper, the faster the discharge is, the more residual material remained in the hopper. Table 13 sums up the measured residuals in the hopper after discharge.

Table 13: Results of residual sample mass in the hopper measured for hopper discharge pre-tests (n.m.: not measurable)

	Emptying speed	Residual sample mass [g]
Hopper 3	fast	n.m.
	very fast	n.m.
Hopper 1	slow	20,0
	fast	21,4
	fast	39,0

Table 14: Residuals in the different hoppers after discharge



3.3.3 Experimental study with selected parameters

3.3.3.1 Discharge rate and radial offset from hopper central axis

The parameter study in vacuum with different discharge rates and radial offsets from the hopper central axis was performed with 150 g of the lunar regolith simulant NU-LHT-2M (standard particle size distribution) with the setup depicted in Figure 18 A and Figure 19 B. The discharge rates that were investigated are 2 s, 5 s, 10 s, and 15 s. It has to be noted that the discharge rate corresponds to the time needed to completely tilt the shovel by 90°. The time does not necessarily correspond to the time needed to completely discharge the shovel. The time needed to completely discharge the shovel might be shorter than the indicated discharge rate, because the regolith empties out abruptly when the shovel reaches a certain angle. The radial offsets from the hopper central axis investigated in the parameter study are - 20 mm, 0 mm, 20 mm, and 40 mm.

The results in Table 15 and Figure 21 show that for the flat hopper, the slower the discharge rate is, the less residuals are in the hopper. Slower discharge rates prevent clogging of the hopper and should therefore be aimed for during a mission. Also, the higher the offset from the central axis of the hopper is, the less residuals are in the hopper. When the material is discharged farther away from the centre of the hopper, it has more area to scatter and a longer distance to flow down. This also reduces the probability of clogging. This effect seems to be so important that, when the offset is 40 mm, the amount of residuals in the hopper does not seem to depend on the discharge rate anymore. This means that the possibility to let the material flow down the hopper wall should be used to prevent clogging.

For the hoppers with a wall angle of 45° and 60°, there were no residuals in the hopper independent of the discharge rate and the radial offset. For the use case to prevent clogging of the hopper outlet, a steep hopper should be chosen instead of a flat one. Also, the material should be discharged rather slowly and with an offset from the centre of the hopper.

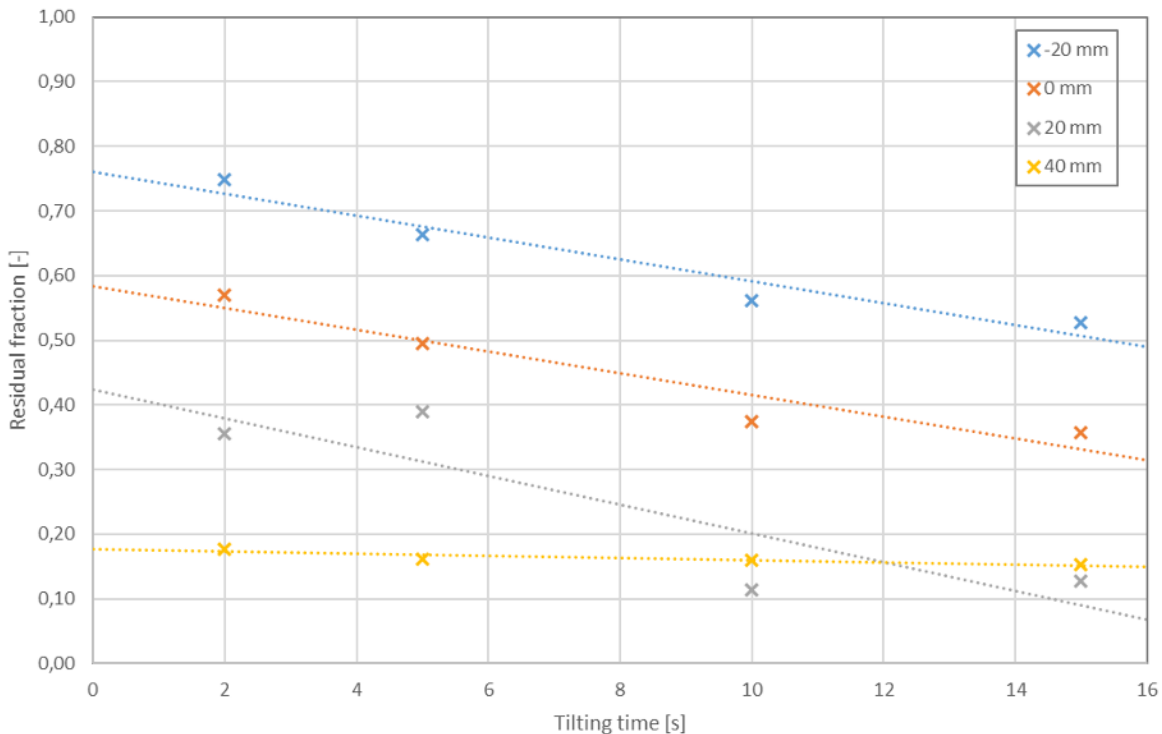


Figure 21: Residual fraction $m_{\text{hopper}}/m_{\text{total}}$ in the flat hopper (hopper 1) plotted over the tilting time of the shovel for different radial offsets from the hopper central axis

Table 15: Residual fraction ($m_{\text{hopper}}/m_{\text{total}}$) in the hopper 1 depending on the tilting time of the shovel and the radial offset from the hopper central axis.

Hopper 1				
Tilting time	Radial offset			
	-20 mm	0 mm	20 mm	40 mm
2 s	0,75	0,57	0,36	0,18
5 s	0,66	0,49	0,39	0,16
10 s	0,56	0,37	0,11	0,16
15 s	0,53	0,36	0,13	0,15

Table 16: Residual fraction ($m_{\text{hopper}}/m_{\text{total}}$) in the hopper 2 depending on the tilting time of the shovel and the radial offset from the hopper central axis.

Hopper 2		
Tilting time	Radial offset	
	0 mm	40 mm
2 s	0,00	0,00
15 s	0,00	0,00

Table 17: Residual fraction ($m_{\text{hopper}}/m_{\text{total}}$) in the hopper 3 depending on the tilting time of the shovel and the radial offset from the hopper central axis.

Hopper 3		
Tilting time	Radial offset	
	0 mm	40 mm
2 s	0,00	0,00
15 s	0,00	0,00

3.3.3.2 Not axisymmetric setup

The parameter study in vacuum with the not axisymmetric setup was performed with 150 g of the lunar regolith simulant NU-LHT-2M (standard particle size distribution) with the setup depicted in Figure 19 C and Figure 20 B. The steepest hopper (wall angle 60°) was tilted in a way that the lower wall angle reached values of 30°, 35°, 40°, 45°, and 50°. Results are summarized in Table 18.

In general, as for the axisymmetric setup, there are less residuals in the hopper the steeper the hopper wall is. During the measurement with the 35° lower wall angle, the hopper output clogged completely so that nearly half of the material remained in the hopper. For small lower wall angles, there is a high risk of clogging with a not axisymmetric setup. For a lower wall angle of 45°, the result is marginally poorer than for the axisymmetric setup with the 45° steep hopper. This shows that the tilted setup negatively affects the material flow in the hopper. For a lower wall angle of 50° or higher, the axisymmetry does not affect the amount of residuals in the hopper anymore.

Table 18: Residual fraction ($m_{\text{hopper}}/m_{\text{total}}$) in the hopper 3 depending on the lower wall angle in relation to horizontal.

		Lower wall angle				
		30°	35°	40°	45°	50°
Fraction	0,195	0,450	0,179	0,003	0,000	

3.3.3.3 Ungrounded vs grounded setup

The parameter study in vacuum with the ungrounded setup was performed with 150 g of the lunar regolith simulant NU-LHT-2M (standard particle size distribution) with the setup depicted in Figure 18 B and Figure 19 B. The hopper was connected to the grounded vacuum chamber. Discharge rates of 2 s and 15 s were investigated for the 30° steep hopper. The radial offset of 0 mm was investigated. For each modulation, three test runs were performed in order to evaluate the error. Results are summarized in Table 19 and plotted in Figure 22.

In contradiction to expectations, the grounded setup showed poorer results (mean value of residuals in the hopper) than the corresponding measurements with the ungrounded setup for a discharge rate of 2 s. For a slow discharge rate, the mean value of residuals in the hopper is similar for both setups. However, the error bars (see Figure 22) are nearer for the grounded setup, thus the results might be more repeatable than for the not grounded setup. The error is relatively large, therefore no distinct difference between the grounded and the not grounded setup can be discerned. This might be due to the choice of material (stainless steel) that was made because of its low susceptibility of triboelectric charging. Hence, there is probably no or no significant difference in built-up triboelectric charges between the two setups.

Table 19: Residual fraction ($m_{\text{hopper}}/m_{\text{total}}$) in the hopper 1 depending on the tilting time of the shovel. Results from both grounded and not grounded setup can be compared.

Hopper 30°		Not grounded				Grounded			
		0mm	0mm	0mm	Mean value	0mm	0mm	0mm	Mean value
2s	m_Hopper [g]	93,51	31,41	99,58	74,83	95,61	88,24	88,08	90,64
	m_total [g]	149,94	149,74	149,82	149,83	150,06	150,02	149,98	150,02
	Fraction	0,62	0,21	0,66	0,50	0,64	0,59	0,59	0,60
15s	m_Hopper [g]	86,16	27,24	93,91	69,10	73,10	66,08	68,07	69,08
	m_total [g]	149,88	150,17	149,91	149,99	150,07	150,04	149,95	150,02
	Fraction	0,57	0,18	0,63	0,46	0,49	0,44	0,45	0,46

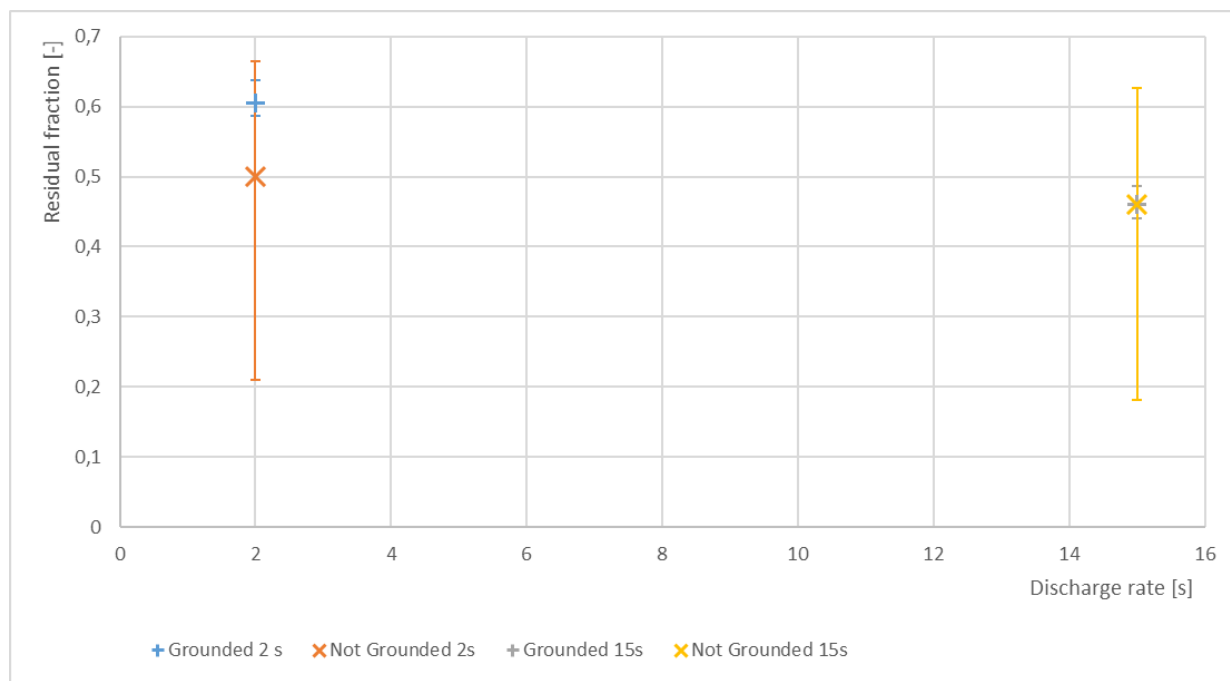


Figure 22: Mean residual fraction value of the grounded and not grounded setup with error bars in the flat hopper depending on the discharge rate.

3.4 Simulant characterisation

3.4.1 Particle size distribution analysis of unprocessed

Particle size distribution of the simulant has been measured at the TUM Chair of Energy Systems both with laser diffraction analysis and with dynamic image analysis. Laser diffraction analysis has a measuring range between 0.03 µm and 1 mm and requires approximately 200 mg of sample for a single determination. Dynamic image analysis detects particle sizes between 0.8 µm and 8 mm and requires maximum a teaspoonful of sample (depending on the sample). Unlike the laser diffraction analysis, the imaging analysis can not only determine the particle size distribution of a sample but also the particle shape (sphericity, symmetry, width/length ratio).

For laser diffraction analysis, 10 samples were measured and the average was calculated. For dynamic image analysis, triple determination was performed and the average was calculated. Particle sizes of dynamic image analysis are based on the minimum chord of the particles, thus the results are comparable to sieve analysis. Table 20 summarizes important values of NU-LHT-2M determined with dynamic image analysis. Figure 23 depicts the particle size distributions of NU-LHT-2M measured by TUM and Zeng et al. (2010) and of lunar soil average.

Table 20: Important values for NU-LHT-2M determined with dynamic image analysis and laser diffraction

Property	Dynamic image analysis	Laser diffraction
Mean diameter [μm]	252.3	n/a
Diameter [μm] at Q3 = 10.0 %	50.8	3.5
Diameter [μm] at Q3 = 50.0 %	169.5	59.5
Diameter [μm] at Q3 = 90.0 %	548.2	277.9
Mean sphericity	0.80	n/a
Mean symmetry	0.88	n/a
Mean width/length	0.68	n/a

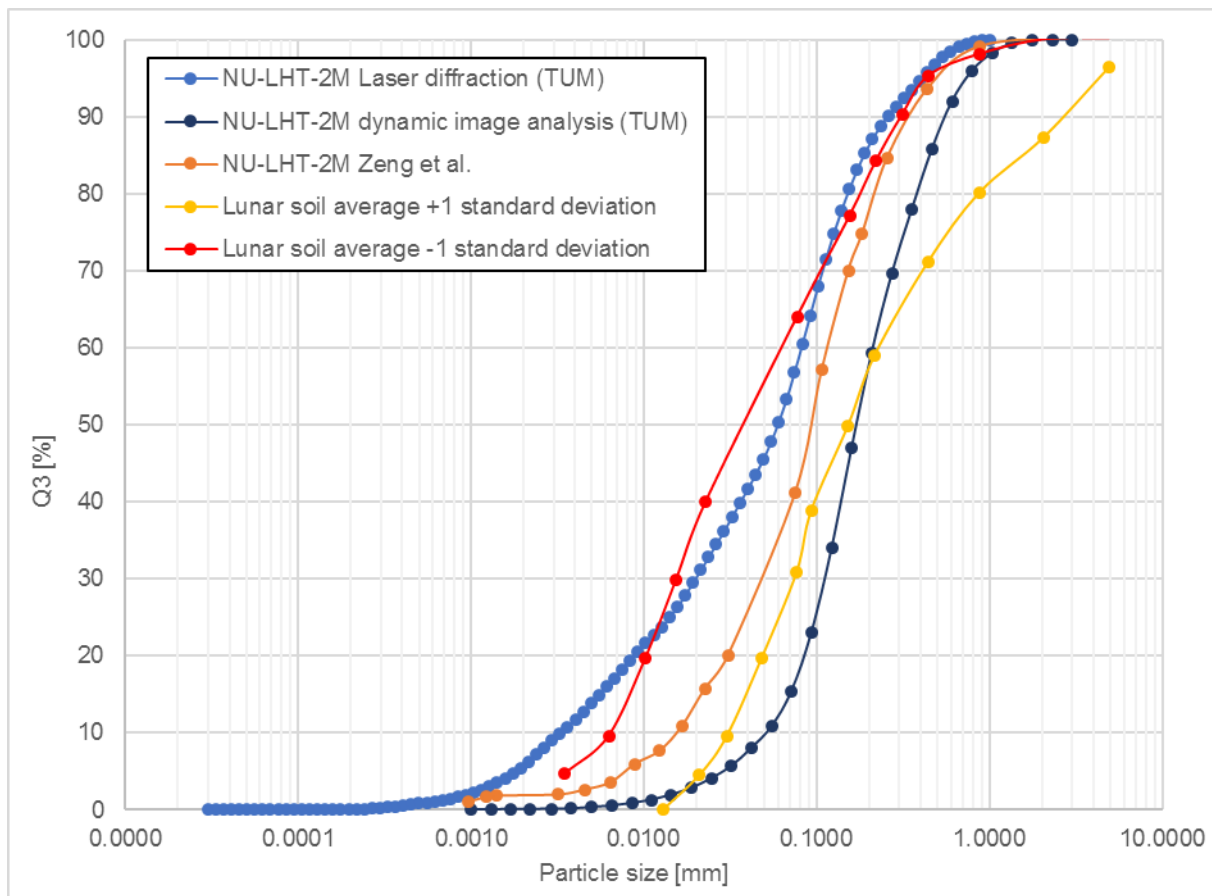


Figure 23: Particle size distribution of NU-LHT-2M measured by TUM and Zeng et al. (Zeng, He and Wilkinson, 2010) and of lunar soil average adopted from Zeng et al. (Zeng, He and Wilkinson, 2010).

3.4.2 Shear tests of unprocessed and processed material

Shear/penetration tests have not yet been started due to the unavailability of larger amounts of the lunar regolith simulant NU-LHT-2M. As soon as a sufficient quantity (500 cm³ to 1500 cm³) has been provided by the customer, the tests will be conducted at the TUM Chair of Process Systems Engineering as described in the proposal.

4 Design considerations for lunar environment

The aim of this work is to present a regolith handling system suitable for lunar applications including a vibrated conveyer to convey regolith into a potential ISRU reactor and a hopper feeding regolith from a shovel onto the conveyer trough. Experiments performed in the frame of the here presented study have been performed under terrestrial gravity and serve as reference to point out potential risks that shall be avoided for later design. In the following, first design considerations for lunar application are deduced from obtained results and literature research. Not only does reduced gravity have a major impact on material behaviour but also its exposure to micrometeorite bombardment and to a high level of radiation in ultrahigh vacuum environment, leading to very adhesive behaviour (Berkebile and Gaier, 2012).

4.1 Hopper design

Several experiments and design considerations for hopper feed systems for lunar applications have been made. Mueller and Townsend (Mueller and Townsend, 2009, no date) have performed parabolic flights at 1/6 g to test their regolith feed hopper for the ROxygen Hydrogen Reduction Reactor System. They used larger quantities than in the here discussed experiments (in the order of several kilograms). For the simulant JSC-1A, it took approximately six times longer for the material to flow through the hopper at 1/6 g than at 1 g. It needed tapping to flow through the hopper. The simulants NU-LHT-2M and OB-1 needed more assistance (bouncing technique at 3 Hz) to flow. Reiss et al. (Reiss et al., 2014) investigated the flow of JSC-1A and NU-LHT-2M in hour-glass-like hopper configurations under reduced gravity. Reduced gravity lead to lower bulk density, lower sample flow rate and higher probability of clogging. In general, higher inclination angles and larger outlet diameters of the hoppers lead to faster sample flow. Walton (Walton, 2012) has discussed the minimum outlet diameter for hopper-like containers and comes to a result of 5-6 cm but without defining geometry and sample mass.

Experiments made in this study confirm previously made observations. To avoid clogging and residuals in the hopper, the hopper wall inclination angles should be at least 60° and the hopper outlet diameter as large as possible. Furthermore, the sample should be filled in the hopper slowly and not at once. Furthermore, it should be poured in the hopper with a radial offset from the hopper central axis. In all experiments, adhesive behaviour of the material could only be marginally taken into account since the behaviour of real lunar regolith on the Moon highly differs from material on Earth. This is why all designs considerations should be made conservatively and e.g. a tapping or vibrating mechanism should be taken into account for the hopper feed system.

4.2 Conveyer design

As already mentioned in section 3.1.1 a), two different forms of transport on a linear conveyer exist: sliding (or slip principle) and oblique hopping (or micro throw principle). In this study, the investigated form of transport is the micro throw principle. The transition from sliding to hopping occurs as soon as the condition

$$\omega^2 \cdot A \cdot \sin\alpha \cdot \sin\omega t > g$$

with ω the oscillation frequency, A the oscillating amplitude, α the inclination angle of driving with respect to the horizontal trough surface and g the gravitational constant, is fulfilled (El Hor et al., 2005).

Assuming that the frequency ω and the inclination angle α are fixed, the reduced gravity on the Moon of 1/6 of terrestrial gravity will have the effect that hopping on the Moon occurs at 1/6th the amplitude at which hopping will first occur on Earth. For rough estimates the assumption can be made that conveying that is feasible on Earth is also feasible on the Moon with 1/6 of the selected amplitude. All conveying modes investigated in this study should therefore in principle be feasible on the Moon. This also applies for upwards transportation with an inclination of 15° and a stroke of 0.3 mm (which was not feasible under lab conditions),

since upwards transportation with an inclination of 15° and a stroke of 0.5 mm was feasible. Therefore, 15° upwards conveying on the Moon could be feasible for strokes <0.1 mm. For more detailed correlation further experiments and modelling and simulation will have to be performed to take into account the influence of further aspects that cannot be neglected, e.g. cohesivity, particle size distribution, particle shape.

Another aspect that has to be considered for lunar applications is uphill transportation, since regolith will most likely be conveyed from about lunar surface to higher above the surface where it will be filled into a reactor. Experiments showed that uphill transportation with a vibratory conveyer has its limits in terms of maximum inclination of the conveyer trough. Furthermore, the longer the trough, the more complicated the designing and operation of the vibratory conveyer will be – e.g. due to higher weight, resonance effects etc. One possibility to avoid those potential problems is a form of uphill conveyer cascade, as depicted in Figure 24. This design has several advantages, not only for uphill transport but also for horizontal transport over longer distances. It allows the designing and testing of only a short conveyer fragment, which can then be stringed together as often as needed. This makes the system flexible and conveying distances can alternate without having to redesign the whole conveying system. Also, material can easily be conveyed along a non-straight path.

An alternative design for uphill conveying of regolith is a conveyer with finlike asperities as described in (Chen et al., 2019). This sawtooth-like texture has the advantage, that the direction of excitation can be longitudinal to the conveying direction, which would be one designing aspect less to consider. The disadvantage is that manufacturing of such a conveyer trough is more complicated and hence more expensive. In general, this kind of conveyer could also be aligned in a cascade as depicted in Figure 24.

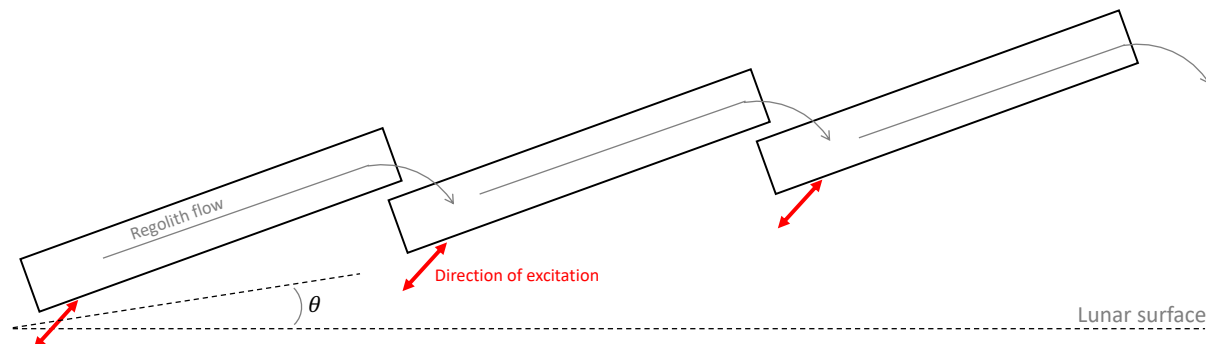


Figure 24: Possible design concept for uphill regolith transportation with multiple vibratory conveyors

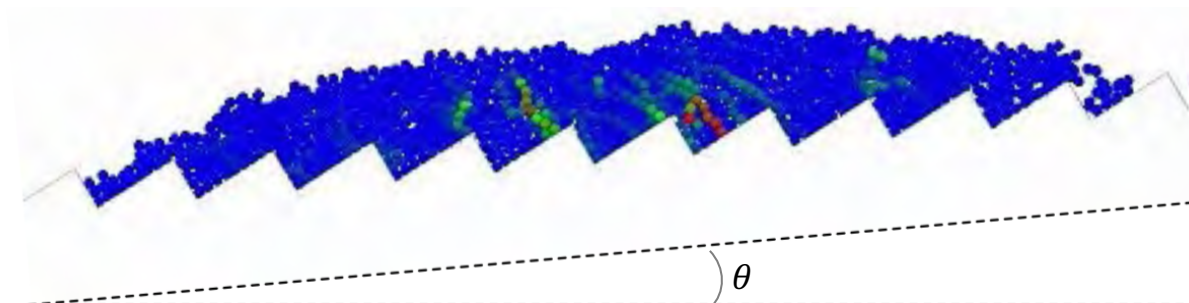


Figure 25: Possible design concept for uphill regolith transportation using a sawtooth texture (figure taken from (Chen et al., 2019))

5 References

- Berkebile, S. and Gaier, J. R. (2012) 'Adhesion in a vacuum environment and its implications for dust mitigation techniques on airless bodies', *Proceedings of the 42nd International Conference on Environmental Systems*, p. AIAA 2012-3465.
- Chen, H. et al. (2019) 'A Vibratory Conveying Method for Planetary Regolith: Preliminary Experiment and Numerical Simulation', *IEEE Access*. IEEE, 7, pp. 29386–29396. doi: 10.1109/ACCESS.2019.2902348.
- Despotović, Ž. V. et al. (2017) 'Mathematical modeling of resonant linear vibratory conveyor with electromagnetic excitation: simulations and experimental results', *Applied Mathematical Modelling*, 41, pp. 1–24. doi: 10.1016/j.apm.2016.09.010.
- El Hor, H. et al. (2005) 'Model for transport of granular matter on vibratory conveyors', *Powders and Grains 2005 - Proceedings of the 5th International Conference on Micromechanics of Granular Media*, 2(1), pp. 1191–1195.
- Mueller, P. and Townsend, I. I. (no date) 'Lunar Regolith Simulant Feed System for a Hydrogen Reduction Reactor System'. Available at: <https://ntrs.nasa.gov/archive/nasa/casi.ntrs.nasa.gov/20110011479.pdf> (Accessed: 24 May 2018).
- Mueller, R. P. and Townsend, I. (2009) 'Effects of Regolith Simulant Properties on an Experiment: ROxygen Phase I Input Hopper Reduced Gravity Flight - Houston, TX', *Lunar Regolith / Simulant Workshop*. Huntsville. Available at: <https://www.yumpu.com/en/document/read/6104777/effects-of-regolith-simulant-properties-on-an-experiment-ro-ph-i-i-t-> (Accessed: 23 February 2020).
- Nendel, K. and Risch, T. (2010) 'Two-dimensional movement patterns of vibratory conveyors', *Logistics Journal Referierte Veröffentlichungen*, pp. 1–11. doi: 10.2195/LJ_Nendel_Risch_2672.
- Rahmatian, L. A. and Metzger, P. T. (2010) *Soil Test Apparatus for Lunar Surfaces*.
- Reiss, P. et al. (2014) 'Flowability of lunar regolith simulants under reduced gravity and vacuum in hopper-based conveying devices', *Journal of Terramechanics*, 55, pp. 61–72. doi: 10.1016/j.jterra.2014.04.005.
- Walton, O. (2012) 'Challenges in transporting, handling and processing regolith in the lunar environment', in Badescu, V. (ed.) *Moon*. Springer Berlin Heidelberg, pp. 267–293. doi: 10.1007/978-3-642-27969-0.
- Zeng, X., He, C. and Wilkinson, A. (2010) 'Geotechnical properties of NU-LHT-2M lunar highland simulant', *Journal of Aerospace Engineering*, 23(4), pp. 213–218. doi: 10.1061/?ASCE?AS.1943-5525.0000026 CE.
- Zhao, Y., Huang, F. and Zhao, Z. (2013) 'Dynamic Analysis On Vertical Vibratory Conveyor'. doi: 10.4028/www.scientific.net/AMR.694-697.3.